

ADAPTIVE MESH METHODS FOR ELASTOHYDRODYNAMIC LUBRICATION

Christopher E. Goodyer*, **Roger Fairlie***, **Martin Berzins***
and **Laurence E. Scales[†]**

*Computational PDEs Unit, School of Computing, University of Leeds, LS2 9JT, UK e-mail:
ceg@comp.leeds.ac.uk, web page: <http://www.comp.leeds.ac.uk/cpde/>

[†]Shell Global Solutions, Cheshire Innovation Park, P.O. Box 1, Chester, CH1 3SH, UK

Key words: Elastohydrodynamic lubrication, Multigrid, Adaptive meshing

Abstract. *The solution of elastohydrodynamic lubrication problems is both computationally intensive and industrially relevant. Although the use of fast multilevel techniques makes it possible to solve standard EHL problems quickly, there is a need to use much finer meshes to resolve features such as surface roughness. In this paper we investigate the use of adaptive meshing in order to focus computational work only on those parts of the solution domain where high resolution of grid points is necessary. The results show that mesh adaptation reduces the computational cost while maintaining the quality of the solution.*

1 INTRODUCTION

Inside an engine there are many components in continuous relative motion. Lubricants are introduced to separate the surfaces, and hence reduce the frictional force which would otherwise cause large amounts of wear. For example, journal bearings and gears experience a very large applied pressure over a very small contact area. The maximum pressure in these contacts can reach up to about 3 GPa (i.e. 3×10^9 Pascals). At such a great pressure, deformation of the contacting surfaces occurs. This situation is called *Elastohydrodynamic lubrication* (EHL).

The range of scales in EHL problems is great; loads in the order of giga-Pascals applied across contacts with a minimum film thickness in the micrometre range with lubricant molecules passing through the contact in a hundredth of a second.

Numerical simulations of EHL problems are important for the design of both components and lubricants. Inside the contact the large pressure range means that a compressible lubricant model must be used, since there are large changes in both the density and viscosity of the lubricant. Increasingly realistic rheological models are being combined with thermal characteristics in order to attempt to accurately capture the true physical behaviour. Such models lead to highly non-linear differential equations which require special numerical techniques.

The key numerical methods used in EHL solvers are the multigrid method [1] and multilevel multi-integration [2], which have proved robust and highly desirable in terms of reducing the time spent in solving EHL problems.

There is still, however, a continuing drive to improve the efficiency and applicability of solvers for EHL problems. This is arising from a number of issues. First, fluid effects are important in cutting edge industrial applications and there is therefore a need to capture the correct rheology of the lubricant [3]. Determination of the rheological parameters of a fluid by fitting experimental measurements of various kinds is an optimisation problem requiring many thousands of EHL solutions to be computed and hence efficiency is a major issue. Second, accurate solutions of micro-EHL problems (which are generally also transient) with realistic surface roughness requires such a high spatial resolution that even a single solution may be a large computational task [4].

In this paper we investigate ways of decreasing the computational effort to achieve accurate solutions to point contact EHL problems, particularly by use of spatial adaptivity. The goal is to find a balance between speed and accuracy. The potential benefits of using grid refinement, especially for the micro-EHL problem, are enormous. In these cases the effects of low amplitude surface defects or roughness dramatically alters the solution profile. Adaptive meshing for EHL problems has only been used in [5, 6] and very little explanation of the methods used was given. We will give details of various different methods for deciding how to refine the computational domain, and explain how this fits inside the EHL multigrid framework. Results will be presented showing how significant speed-ups can be achieved without losing solution accuracy.

The rest of this paper is made up as follows. In Section 2 the equations governing the EHL system will be presented. The numerical techniques used to solve them will be briefly outlined in Section 3, including a description of the multilevel techniques applied. The methods

chosen for grid adaptation will be presented in Section 4 along with results showing the comparative accuracies and potential speed-ups of the methods used. The paper will be concluded in Section 5.

2 EQUATIONS

The EHL problem is governed by the relationship between the pressure distribution across the contact, and the deformation of the contacts caused by this pressure distribution. The pressure distribution is also governed by the physical properties of the lubricant under consideration. In this work only generalised Newtonian models will be considered, and the example cases will be isothermal circular point contact cases. This represents the lubrication of two three-dimensional spherical surfaces. By reduction of the geometry these are represented by solving the problem of a rotating ball on a plane, with lubricant flow between them. Since the separation of the surfaces is very small, for generalised Newtonian lubricant rheologies, the problem will not require solving in the direction normal to the surface plane [7].

The pressure distribution is described by the Reynolds Equation [8]. By first defining a non-dimensional quantity, ε by:

$$\varepsilon = \frac{\bar{\rho}H^3}{\bar{\eta}\lambda}, \quad (1)$$

then the Reynolds Equation to be used for the point contact case is given, in non-dimensional form, by:

$$\frac{\partial}{\partial X} \left(\varepsilon \frac{\partial P}{\partial X} \right) + \frac{\partial}{\partial Y} \left(\varepsilon \frac{\partial P}{\partial Y} \right) - \frac{u_s(T)}{u_s(0)} \frac{\partial(\bar{\rho}H)}{\partial X} - \frac{\partial(\bar{\rho}H)}{\partial T} = 0. \quad (2)$$

where P is the non-dimensionalised pressure

H is the non-dimensionalised film thickness

$\bar{\rho}$ is the non-dimensional density of the lubricant

$\bar{\eta}$ is the non-dimensional viscosity of the lubricant

u_s is the sum of the speeds of the two surfaces in X -direction at time T

λ is a non-dimensional constant

X, Y are the non-dimensional coordinate directions

and T is the non-dimensional time.

Non-dimensionalisation of the equations means that the contact has unit Hertzian radius, and that the maximum Hertzian pressure is represented by $P = 1$.

The boundary conditions for pressure are such that all exterior boundaries are considered to be sufficiently distant to represent infinite conditions of having $P = 0$. For the outflow boundary, once the lubricant has passed through the centre of the contact it will form a free boundary, the *cavitation boundary* beyond which there is no lubricant.

The film thickness, H , represents the geometry of the ball, and is given, in non-dimensional form, by:

$$H(X, Y) = H_{00} + \frac{X^2}{2} + \frac{Y^2}{2} + \frac{2}{\pi^2} \int_{-\infty}^{\infty} \int_{-\infty}^{\infty} \frac{P(X', Y') dX' dY'}{\sqrt{(X - X')^2 + (Y - Y')^2}}, \quad (3)$$

where H_{00} is the central offset film thickness, which defines the relative positions of the surfaces if no deformation was to occur. The two parabolic terms represent the undeformed shape of the surface, and the double integral defines the deformation on the surface due to the pressure distribution across the entire domain.

The conservation law for the applied force is called the Force Balance Equation and is given by:

$$\int_{-\infty}^{\infty} \int_{-\infty}^{\infty} P(X, Y) dXdY = \frac{2\pi}{3}. \quad (4)$$

Since an isothermal, generalised Newtonian lubricant model is being used, only expressions for the density and viscosity will be required. The density model chosen is that of Dowson and Higginson [7], which takes into account the compressibility of the lubricant:

$$\bar{\rho}(P) = \frac{0.59 \times 10^9 + 1.34p_h P}{0.59 \times 10^9 + p_h P}, \quad (5)$$

where p_h is the maximum Hertzian pressure.

The viscosity used is governed by the Roelands pressure-viscosity relation [9], a modification of the exponential Barus equation [10], to give more accurate results up to 1 G Pa:

$$\bar{\eta}(P) = e^{\left\{ \frac{\alpha p_0}{z} \left[-1 + \left(1 + \frac{p_h P}{p_0} \right)^z \right] \right\}}, \quad (6)$$

where η_0 is the viscosity at ambient pressure
 p_0 is a constant (typically 1.98×10^8)
 z is the pressure viscosity index, taken as $z = 0.68$
 and α is the pressure viscosity coefficient.

3 NUMERICAL TECHNIQUES

3.1 Solution scheme

The point contact EHL solver described here uses a regular mesh of size $N \times N$ elements, where $N = 2^k + 1$. The level of refinement of the mesh can then be referred to as being grid level k . Due to symmetry about the line $Y = 0$ it is only necessary to solve on half of the computational domain.

Equations (2) to (6) are discretised upon this mesh using standard finite difference techniques, see [11]. The nature of the EHL problem means that there are three very different areas of the domain when calculating pressure. The cavitation region is the area of the solution beyond the free boundary where the Reynolds Equation is not valid, and where pressures are set to be identically zero. In the centre of the domain is the *contact area*, where the pressure rises sharply to reach its maximum peak in a near Hertzian shape. EHL pressure profiles do differ from purely hydrodynamic ones in that there is also the presence of a large ridge on the pressure peak, towards the outflow boundary, as can be seen in Figure 1 where the 3D non-dimensional

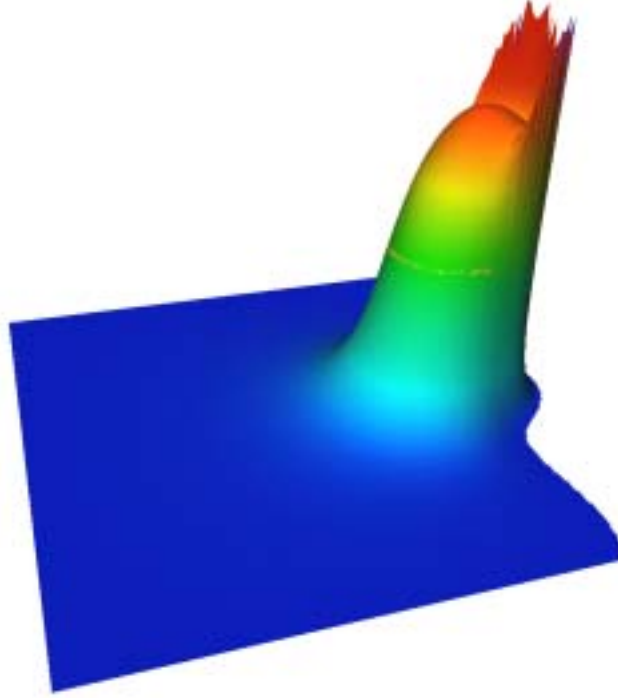


Figure 1: Typical solution for pressure across an EHL point contact

pressure profile is shown. Finally, in the non-contact region the pressure is very small compared to the contact region.

The film thickness calculation, once discretised, has the form:

$$H_{i,j} = H_{00} + \frac{X_i^2}{2} + \frac{Y_j^2}{2} + \sum_{k=1}^{N_x} \sum_{l=1}^{N_y} K_{i,j,k,l} P_{k,l}, \quad (7)$$

where K is the film thickness kernel matrix, approximating the double integral of Equation (3). Hence for every mesh point, (i, j) , the deformation term is a multi-summation of the pressures at all the other points in the computational domain.

The deformation of the surface can be seen in Figure 2 which shows the shape of the contact along the centreline. The deformation away from the original surface geometry is clearly visible, and it can be seen that there is a constriction in the contact towards the outflow, which coincides with a position between the pressure spike and the cavitation boundary.

To calculate the new pressure solution two different relaxation schemes are required in the different pressure positive regions. In the non-contact region a Gauss-Seidel line relaxation scheme is used, whereas in the contact region the Jacobi line relaxation scheme of Nurgat *et al.* [12] is used. The calculation of H_{00} is accomplished by relaxation of the Force Balance

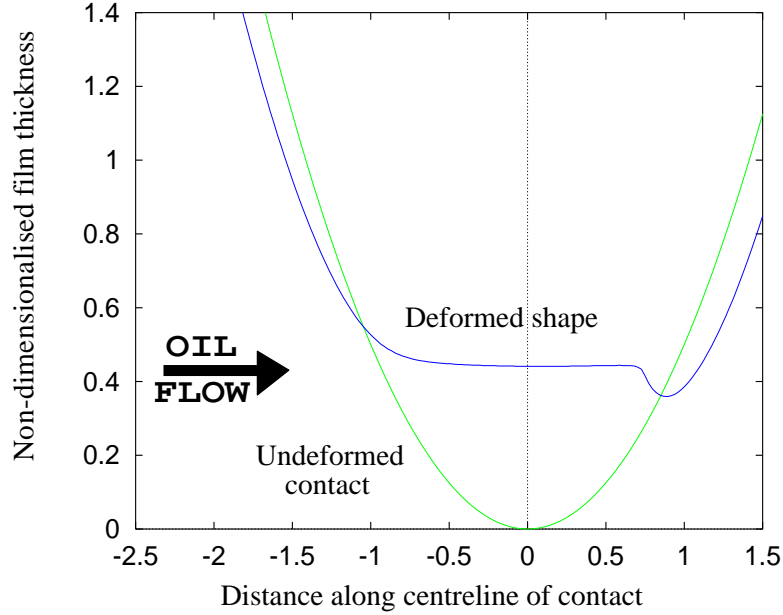


Figure 2: Typical solution for film thickness along the centreline of an EHL point contact

Equation (4), according to:

$$H_{00} \leftarrow H_{00} + c \left(\frac{2\pi}{3} - \Delta X \Delta Y \sum_{i=1}^N \sum_{j=1}^N P_{i,j} \right), \quad (8)$$

for all mesh points (i, j) , where c is a small relaxation parameter.

One smoothing cycle is said to be the sequence of updating all the pressures, $P_{i,j}$, and film thickness values $H_{i,j}$.

3.2 Multilevel techniques

In order to obtain solutions to EHL problems quickly it has proved necessary [1, 13] to use multigrid methods. Multigrid is effective because it uses coarser grid levels to remove errors of different frequencies to those which could be quickly smoothed away on simply the fine grid alone.

The EHL problem is highly non-linear and hence the Full Approximation Scheme (FAS) must be used, see [14, 15]. In-depth descriptions of how multigrid is applied to EHL problems can be found in [11] and [1]. The effectiveness of these techniques in maintaining the asymptotic convergence rates are shown in both of these works. These methods are briefly summarised here.

In the case of a regular mesh with $2^k + 1$ points in each direction then all the mesh points on grid level $k-1$ are coincident with points on level k . Simple operators can then be defined to transfer solutions between adjacent grids, either by injection or weighted interpolation of

neighbouring points. Consider the system

$$\mathcal{L}^k \underline{u}^k = f^k, \quad (9)$$

where \mathcal{L}^k is a discrete approximation to the differential operator \mathcal{L} , and \underline{u}^k approximates a vector of exact solution values \underline{u} , separated by distance δx^k .

At any particular stage, a solution vector \tilde{u}^k will have been calculated, with an error, \underline{e}^k , such that

$$\underline{u}^k = \tilde{u}^k + \underline{e}^k. \quad (10)$$

The solution is relaxed iteratively to obtain new solutions with the aim of reducing this error to below some pre-specified tolerance level.

The single grid relaxation schemes, or smoothers, used to solve EHL problems are very effective at reducing high frequency errors [13, 14] but very slow at reducing low frequency errors. Given that the smoother is able to reduce errors of the frequency of the grid size, then lower frequency errors can be reduced in a multigrid method by use of a (coarser) grid with similar order to that of the error.

From Equation (9) the residual, r^k , of the system can be calculated from

$$r^k = f^k - \mathcal{L}^k \tilde{u}^k, \quad (11)$$

for an approximation \tilde{u}^k to \underline{u}^k . Substituting for f^k from Equation (9) and using Equation (10) enables us to define the residual as

$$r^k = \mathcal{L}^k(\tilde{u}^k + \underline{e}^k) - \mathcal{L}^k \tilde{u}^k, \quad (12)$$

which can be reordered to give

$$\mathcal{L}^k(\tilde{u}^k + \underline{e}^k) = \mathcal{L}^k \tilde{u}^k + r^k. \quad (13)$$

Consider now a coarser grid, grid j . To represent Equation (13) in the same form as (9), i.e.

$$\mathcal{L}^j \hat{u}^j = \hat{f}^j, \quad (14)$$

it is necessary to define \hat{u}^j by

$$\hat{u}^j = I_k^j \tilde{u}^k + \underline{e}^j. \quad (15)$$

The term \hat{f}^j in Equation (14) is called the *FAS right hand side*, and is given by

$$\hat{f}^j = \mathcal{L}^j(I_k^j \tilde{u}^k) + I_k^j r^k, \quad (16)$$

and I_k^j is an inter-grid transfer operator from grid k to grid j .

The solution \hat{u}^j to Equation (14) can be approximated by \bar{u}^j which can then be used to calculate the coarse grid approximation to the error by

$$\tilde{e}^j = \bar{u}^j - I_k^j \tilde{u}^k. \quad (17)$$

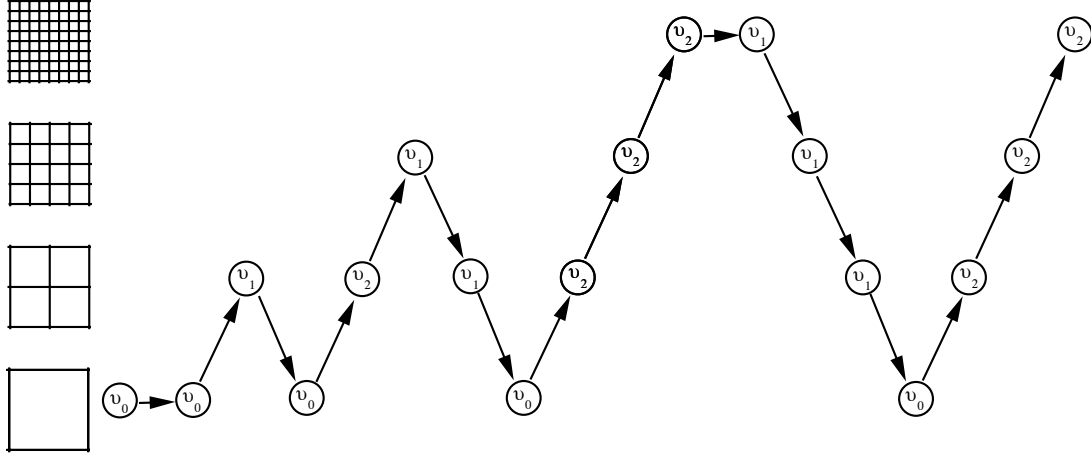


Figure 3: Full multigrid, with one V-cycle per level

This is then used to update the fine grid solution in the following manner:

$$\tilde{\underline{u}}^k \leftarrow \tilde{\underline{u}}^k + I_j^k (\underline{u}^k - I_k^j \tilde{\underline{u}}^k). \quad (18)$$

Assuming that the same iterative process can be used to solve the coarse grid system as the fine grid system, then the finest grid will be used to smooth the highest frequency errors, and progressively coarser grids used to smooth errors of progressively lower frequencies (coarsening), before returning to get an updated solution on the finest mesh (prolongation). The relaxation cycles done before coarsening are called *pre-smooths* and those done after prolongation and correction of the solution are referred to as *post-smooths*.

The simplest multigrid cycle is the V-cycle. An initial approximation on the finest grid has v_1 pre-smooths before being coarsened. This is then repeated until the coarsest mesh is reached where v_0 smoothing cycles are done. The solution on the next finer mesh is then corrected according to Equation (18) before having v_2 post-smooths. Again this process is repeated until a corrected, smoothed solution is reached on the finest mesh. This V-cycle is known as a $V(v_1, v_2)$ -cycle. Typical values for v_1 and v_2 are three or less, although v_0 may be much larger in order to obtain a much better coarse grid solution.

The process of *Full Multigrid* (FMG) is designed to eliminate the large errors which would exist on the fine grid, before it is first used, by starting on a less computationally expensive coarse grid. FMG uses the same multigrid techniques and V-cycles as described above, but applied as shown in Figure 3. This example demonstrates just one V-cycle per level, but there will usually be several to obtain a reasonably converged solution. At the end of each set of V-cycles this solution is then prolonged up to a new finest grid.

For EHL problems the multigrid method has to be modified to deal with the free boundary at the edge of the cavitation region. It has been seen that if information is allowed to propagate from the cavitation region into the pressure positive region in the coarsening or prolonging stages, or if the solution on a coarser grid moves the cavitation boundary one coarse mesh

point into the cavitation region, then stalling may occur [16]. This is because the multigrid process could move the fine grid cavitation boundary and hence the solver will reach a point where the fine grid smooths are only able to remove the errors added by the multigrid process. This problem is eliminated by not applying multigrid near the boundary, however the final convergence of the solution on this boundary will be slower since only fine grid relaxations will be used there.

The other major difference in the multigrid EHL solver is concerned with the iteration for H_{00} , and hence updating the Force Balance Equation (4). This value of H_{00} is only ever corrected once per multigrid cycle, and this is done on the coarsest grid. Appropriate corrections from finer levels are necessary to ensure that it is the applied force on the finest grid which is being conserved, rather than that on coarser grids.

The most computationally expensive part of the solve is that of the calculating the deformation of the surface, due to it being the double sum in Equation (7). Brandt and Lubrecht [2] developed a technique called multilevel multi-integration in order to reduce such a calculation from $\mathcal{O}(N^4)$ to $\mathcal{O}(N^2 \ln N^2)$. This method assumes that outside the neighbourhood of the point being considered, the kernel matrix is smooth enough for a coarse grid representation to be used instead. Inside the neighbourhood of the point, a correction is made to the solution using a summation of all the points in the region.

4 ADAPTIVE MESHING

4.1 Theory

The addition of more fine grid points means that the resolution of the solution can be increased at a cost of solving a larger system of equations. This cost can then dominate the calculation time. However, it may not be necessary to use a fine grid in regions where the solution does not change greatly. The intention of adaptive meshing is to focus the computational work by placing mesh points in the areas of the domain where they are most required for solution accuracy.

The method being applied here is to only use fine grids in selected regions of the domain, see [15] and for EHL problems [11]. In this method only the calculation of the pressure solution is performed on a refined mesh. The film thickness is still evaluated on an unadapted mesh in order to make use of the benefits of multilevel multi-integration.

Considering a three level multigrid formulation then an extra level of refinement may be added over only part of the domain if so desired. This can be seen in Figure 4a where the bottom right hand of the four coarsest squares has been refined. It is possible to just solve for a new finest grid solution using just the points inside the shaded area. The points on the boundary with the unadapted region, namely those marked \bullet and \circ will be treated as Dirichlet. Those outside the shaded region will not be included in the solve. The difference between the two types of boundary points is the accuracy with which they have been obtained. Those marked \bullet are a direct prolongation of the coincident coarser grid point, whilst the hanging nodes, marked by \circ , are only obtained by some interpolation of surrounding coarse grid points.

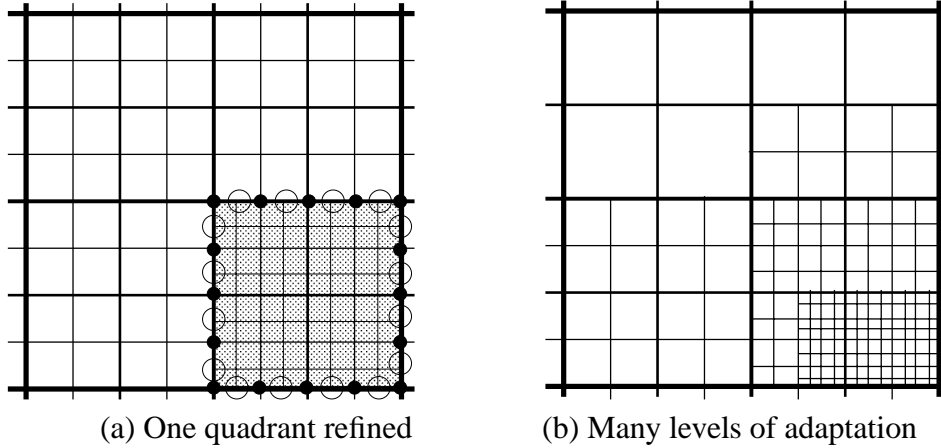


Figure 4: Example of an adapted multigrid mesh

This method fits inside the multigrid framework as follows. Solutions from the finest grid are only generated inside the shaded region, say Ω_{ad} . It is only valid to calculate coarse grid corrections inside this region. Similarly, the calculation of the right hand side functions, previously given in Equation (16), now becomes

$$\hat{f}^j = \begin{cases} \mathcal{L}^j(I_k^j \tilde{u}^k) + I_k^j r^k & (i,j) \in \Omega_{ad} \\ 0 & \text{elsewhere} \end{cases} \quad (19)$$

with all symbols as defined in Section 3.2. Hence it is also the case that on the coarser mesh only those points coincident with points in the adapted mesh should have any knowledge of the presence of finer meshes.

This procedure may be applied iteratively to produce a hierarchy of increasingly refined multigrid meshes. An example of this is shown in Figure 4b which shows five different grid levels with different adaptation domains on each.

It was explained in Section 3.1 that solutions of the EHL system are characterised by three regions of the domain: the contact region, where the pressure is high; the non-contact region, where the pressure is low; and the cavitation region, where the pressure is assumed to be identically zero. In deciding where to adapt the differences between these regions are of great importance.

In the cavitation region there is no reason to use a fine mesh to calculate a non-physical pressure solution which will be set to zero. There must, however, be at least one, and preferably two points, in the cavitation region included to allow the free boundary to adjust its position. An example of adaptation over the free boundary is shown in Figure 5 where the cross-hatched region indicates the area of positive pressure, and the dotted region includes the extra points included into each line solve.

In the rest of the domain there is a lot more freedom about how to choose where to adapt. Deciding the correct refinement criteria is very important to obtaining optimal performance from the use of grid adaptation, however even some crude assumptions will be shown to be very

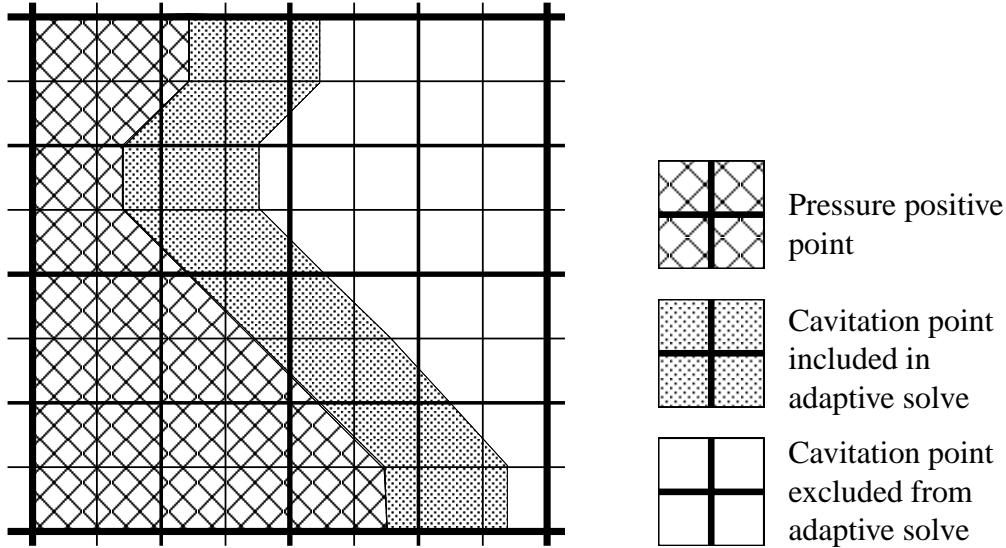


Figure 5: Example showing adaptation around cavitated free boundary

beneficial. There are three possible types of scheme available for deciding on refinement levels; namely arbitrary geometrical decisions, adaptation based on a monitor function, or refinement based on an error test. In the examples below, all three methods will be shown, and their relative effectiveness and applicability judged.

Effective use of the arbitrary geometrical decision scheme relies on *a priori* knowledge of how the solution behaves. In the EHL case this is well defined, since it is known that the high pressure contact region is found inside the unit disc centred at (0,0), that the cavitation region is almost entirely the *X*-positive region not in the contact region, and the non-contact region is the rest of the *X*-negative domain. It is therefore sensible to surmise that refinement in the area of high pressure and great deformation is advisable.

The adaptation can be made more automatic through use of a *monitor function* which will take account of the properties of the solution before deciding which regions need adapting. This idea is similar to the one already commonly used in EHL problems to decide which numerical scheme should be used at individual points, as described in [13]. The monitor function may use solution variables or their derivatives to identify regions of greatest change. In this study the pressure values were used.

Fully automatic refinement can only come through use of an accurate error control function. Much work has been done into grid refinement in many different applications. It is, however, the case that at present no analysis has been done into the error control issues of the EHL problem. In the work of Lubrecht [6] the method of Bai and Brandt [17] was used to decide where to adapt. This uses the quantity τ_k^{k-1} known as the *(k,k-1) relative truncation error* which is the quantity that is to be added to the right hand side of the coarse grid problem, and is thus a measure of the extent to which the local introduction of the finer grid has influenced the global

solution [15]. The test given in [15] is to refine whenever

$$(\Delta X)^k \tau_k^{k-1} < \xi \quad (20)$$

for a chosen tolerance ξ .

4.2 Examples

To test the effectiveness of the grid adaptation, a test case with a maximum Hertzian pressure of 0.45 G Pa was chosen. This was solved on the half-domain $X \in [-4.5, 1.5]$, $Y \in [0, 3]$ using finest meshes between level 5 and level 8, dimensions 65×33 and 513×257 points respectively.

Measuring the accuracy of the results can be done in several different ways. Comparisons can be made between the values of central and minimum film thickness and the height of the pressure spike [11]. For the grid adaptation strategies shown, all of these notable variables are close to those obtained using the corresponding fully fine case. In order to measure differences over all the grid, the L_2 -norm of the differences between solutions on adapted and unadapted grids, for both pressure and film thickness, is used as given by

$$\|u_{ref} - u_{ad}\|_2 = \int_{Y_{min}}^{Y_{max}} \int_{X_{min}}^{X_{max}} (u_{ref} - u_{ad})^2 dX dY \quad (21)$$

where u_{ref} is the reference solution against which the adapted solution, u_{ad} , is compared. The accuracy desired is that the solution of an adapted grid on level k should be significantly closer to the results obtained on an unadapted level k than those obtained on an unadapted level $k-1$ mesh, or coarser.

Comparison between grid levels does, however, rely upon the numerical solution to the equations being similar. Around the pressure spike this need not be the case. The effect of grid spacing for line contact cases has been investigated for many years, and results up to level 10 were shown using adaptivity in the work of Lubrecht [6] and Breukink [18]. Recent work done by the authors into the line contact case has shown that the numerical solution does converge to a well defined pressure spike, however this requires the number of points to increase by several order of magnitude. Unfortunately it was found that small differences in the spike height causes a much greater variation in the film thickness profile.

The different adaptation schemes tested are shown in Table 1, where the major of the test case identifier refers to the finest grid used in the multigrid cycle. Cases 5.0, 6.0, 7.0 and 8.0 use a fixed unadapted mesh. All grid adaptation schemes also include the refinement of the cavitation region as described above. For both the spatial and the pressure based grid adaptation schemes, the refinement on a grid also includes the corresponding refinement described for the next coarser grid. Case 8.1 is the exception to this, with it having been refined on grid 7 for $X < -3$, $Y > 1.5$, and on grid 6 for $X < -3.5$, $Y > 2$.

The L_2 -norm results for comparison between the non-dimensional solutions of pressure between the adaptive, and fully fine, fully converged, comparison cases are shown in Table 2. Since these tables show the difference between adapted solutions and unadapted cases, the

Finest grid level	Spatially adapted	Pressure refinement	τ_k^{k-1} test refinement
6	<i>Case 6.1</i> $X < -3.5, Y > 2.25$	<i>Case 6.2</i> $P > 2 \times 10^{-3}$	<i>Case 6.3</i> $\xi = 1 \times 10^{-6}$
7	<i>Case 7.1</i> $X < -1.5, Y > 1$	<i>Case 7.2</i> $P > 5 \times 10^{-2}$	<i>Case 7.3</i> $\xi = 1 \times 10^{-6}$
8	<i>Case 8.1</i> $X < -2.25, Y > 0.95$	<i>Case 8.2</i> $P > 1 \times 10^{-1}$	<i>Case 8.3</i> $\xi = 1 \times 10^{-7}$

Table 1: Adaptivity schemes used for the grid adaptivity tests

smaller the L_2 -norm, the closer the solutions. It can clearly be seen that the results are closest to results on the same finest fixed grid level. As expected, the results for pressure do seem more accurate than those for film thickness, against either finer or coarser meshes. This difference is due to the difference in the pressure solutions only lying in the resolution of the pressure ridge, while the global nature of the deformation calculation, equation (3), means that any pressure differences here are propagated throughout the entire film thickness solution.

Finally, in Table 3, computational timings are shown for each case. These show that solutions on adapted grids can be computed significantly faster than in the unadapted case, often up to around half the time. This means that results of significantly greater accuracy than those on grid k , say, can be computed on grid $k+1$ in roughly only twice the time, rather than the factor of four for unadapted cases.

5 CONCLUSIONS AND FUTURE WORK

In this paper we have examined some of the benefits of applying adaptive methods to elasto-hydrodynamic lubrication problems.

Grid adaptivity has been successfully applied. Selection of areas of the mesh where solutions are relatively smooth allows a reduced domain to be considered for the solution of the equations on the finest mesh. By applying increasingly large regions of refinement on decreasing levels in the multigrid hierarchy the computational effort on the finest meshes can be directed only to the areas of the solution domain where it would be most beneficial. Three different schemes for deciding where to refine were evaluated for a steady state example. The computational time was typically reduced by a half, without a significant drop in accuracy, and solutions were still the same order of accuracy better than those on any coarser mesh, and of the same quality when compared against unadapted solutions on finer grid levels.

Pressure

	Compared against case			
	8.0	7.0	6.0	5.0
6.1	9.66×10^{-3}	4.40×10^{-3}	1.07×10^{-5}	8.88×10^{-3}
6.2	1.02×10^{-2}	4.80×10^{-3}	3.89×10^{-5}	8.41×10^{-3}
6.3	2.98×10^{-2}	1.89×10^{-2}	1.53×10^{-7}	8.57×10^{-3}
7.1	3.13×10^{-3}	1.75×10^{-4}	4.32×10^{-3}	1.78×10^{-2}
7.2	3.43×10^{-3}	2.44×10^{-4}	4.12×10^{-3}	1.75×10^{-2}
7.3	8.17×10^{-3}	2.12×10^{-4}	4.19×10^{-3}	1.76×10^{-2}
8.1	1.44×10^{-5}	2.27×10^{-3}	9.76×10^{-3}	2.41×10^{-2}
8.2	7.35×10^{-5}	1.99×10^{-3}	9.33×10^{-3}	2.36×10^{-2}
8.3	2.19×10^{-5}	2.54×10^{-3}	1.02×10^{-2}	2.46×10^{-2}

Film thickness

	Compared against case			
	8.0	7.0	6.0	5.0
6.1	2.28×10^{-1}	2.42×10^{-1}	5.04×10^{-6}	4.88×10^{-1}
6.2	2.29×10^{-1}	2.43×10^{-1}	1.38×10^{-5}	4.87×10^{-1}
6.3	2.31×10^{-1}	2.49×10^{-1}	5.11×10^{-9}	4.87×10^{-1}
7.1	1.21×10^{-1}	7.27×10^{-5}	2.42×10^{-1}	4.58×10^{-1}
7.2	1.21×10^{-1}	1.45×10^{-4}	2.42×10^{-1}	4.58×10^{-1}
7.3	1.21×10^{-1}	1.07×10^{-4}	2.42×10^{-1}	4.58×10^{-1}
8.1	3.15×10^{-5}	1.21×10^{-1}	2.28×10^{-1}	4.20×10^{-1}
8.2	1.97×10^{-4}	1.21×10^{-1}	2.27×10^{-1}	4.19×10^{-1}
8.3	6.63×10^{-6}	1.21×10^{-1}	2.28×10^{-1}	4.21×10^{-1}

Table 2: L_2 -norms of differences in non-dimensionalised pressure and film thickness between adapted and un-adapted cases on grids 6 to 8

Case	Time for 10 iterations (s)	Saving on unadapted case (s)	Percentage time saved
6.1	19.5	11.8	37.7
6.2	20.5	10.8	34.6
6.3	30.4	1.0	3.1
7.1	56.0	61.2	52.2
7.2	58.7	58.4	49.9
7.3	80.9	36.3	31.0
8.1	237	245	51.3
8.2	218	264	55.6
8.3	276	206	44.3

Table 3: Computational timings for 10 multigrid V-cycles for adaptation test cases

In addition to using these techniques to tackle harder, and more realistic problems. The grid adaptation strategy presented above is only based on reducing the order of calculation of the pressure solution. For a fully adaptive strategy, the film thickness calculation will also need refinement. A strategy for multilevel multi-integration on adaptive grids has been proposed by Brandt and Venner [19], and using this, or similar, is an obvious progression.

Adaptation need not be restricted to only being applied spatially. The method of variable timestepping for EHL problems, introduced by the authors in [20] has been further developed in [11]. Results have been presented showing significant savings in computational work to achieve results of the same accuracy as traditional fixed timestep methods.

REFERENCES

- [1] C. H. Venner and A. A. Lubrecht. *Multilevel Methods in Lubrication*. Elsevier, 2000.
- [2] A. Brandt and A. A. Lubrecht. Multilevel matrix multiplication and fast solution of integral equations. *Journal of Computational Physics*, 90(2):348–370, 1990.
- [3] L. E. Scales. Quantifying the rheological basis of traction fluid performance. In *Proceedings of the SAE International Fuels and Lubricants Meeting, Toronto, Canada*. Society of Automotive Engineers, 1999.
- [4] A. A. Lubrecht and C. H. Venner. Elastohydrodynamic lubrication of rough surfaces. *Proceedings of the Institution of Mechanical Engineers Part J, Journal of Engineering Tribology*, 213:397–403, 1999.
- [5] A. A. Lubrecht, C. H. Venner, W. E. ten Napel, and R. Bosma. Film thickness calculations in elastohydrodynamically lubricated circular contacts, using a multigrid method. *Trans. ASME, Journal of Tribology*, 110:503–507, 1988.
- [6] A. A. Lubrecht. *Numerical solution of the EHL line and point contact problem using multigrid techniques*. PhD thesis, University of Twente, Enschede, The Netherlands, 1987. ISBN 90-9001583-3.
- [7] D. Dowson and G. R. Higginson. *Elasto-hydrodynamic Lubrication, The Fundamentals of Roller and Gear Lubrication*. Pergamon Press, Oxford, Great Britain, 1966.
- [8] O. Reynolds. On the theory of lubrication and its application to Mr Beauchamp Tower’s experiments, including an experimental determination of the viscosity of olive oil. *Philosophical Transactions of the Royal Society of London*, 177:157–234, 1886.
- [9] C. J. A. Roelands. *Correlational Aspects of the viscosity-temperature-pressure relationship of lubricating oils*. PhD thesis, Technische Hogeschool Delft, The Netherlands, 1966.
- [10] C. Barus. Isothermals, isopiestic and isometrics relative to viscosity. *American Journal of Science*, 45:87–96, 1893.
- [11] C. E. Goodyer. *Adaptive Numerical Methods for Elastohydrodynamic Lubrication*. PhD thesis, University of Leeds, Leeds, England, 2001.
- [12] E. Nurgat, M. Berzins, and L. E. Scales. Solving EHL problems using iterative, multigrid and homotopy methods. *Trans. ASME, Journal of Tribology*, 121(1):28–34, 1999.
- [13] C. H. Venner. *Multilevel Solution of the EHL Line and Point Contact Problems*. PhD thesis, University of Twente, Enschede, The Netherlands, 1991. ISBN 90-9003974-0.
- [14] W. L. Briggs. *A Multigrid Tutorial, second edition*. SIAM, 2000.

- [15] U. Trottenberg, C. Oosterlee, and A. Schüller. *Multigrid*. Academic Press, 2001.
- [16] C. E. Goodyer, R. Fairlie, M. Berzins, and L. E. Scales. An in-depth investigation of the multigrid approach for steady and transient EHL problems. In D. Dowson *et al.*, editor, *Thinning films and Tribological Interfaces, Proceedings of the 26th Leeds-Lyon Symposium on Tribology*, pages 95–102. Elsevier, 2000.
- [17] D. Bai and A. Brandt. Local mesh refinement multigrid techniques. *SIAM Journal on Scientific and Statistical Computing*, 8(2):109–134, 1987.
- [18] G. A. C. Breukink. Het oplossen van het Elastohydrodynamische smeringsprobleem gebruikmakend van multigrid. Master’s thesis, University of Twente, Enschede, The Netherlands, 1986. (In Dutch).
- [19] A. Brandt and C. H. Venner. Multilevel evaluation of integral transforms on adaptive grids. Technical Report WI/GC-5, Weizmann Institute of Science, 1996.
- [20] C. E. Goodyer, R. Fairlie, M. Berzins, and L. E. Scales. Adaptive techniques for elastohydrodynamic lubrication solvers. In G. Dalmaz *et al.*, editor, *Tribology Research: From Model Experiment to Industrial Problem, Proceedings of the 27th Leeds-Lyon Symposium on Tribology*. Elsevier, 2001.